

Studies of Active Galactic Nuclei with the VLT Interferometer

Klaus Meisenheimer

*Max-Planck-Institut für Astronomie,
Königstuhl 17, D-69117 Heidelberg, Germany*

Abstract

The observation of extragalactic targets is the most challenging program for interferometric instruments operating at infrared wavelengths. Of them, only the nearest Active Galactic Nuclei (AGN) are bright enough to be reached with the current instruments at the VLT Interferometer (VLTI). So far, two Seyfert galaxies, NGC 1068 and the Circinus galaxy, have been studied in detail with the MID-infrared Interferometric instrument (MIDI). First results could also be obtained for the nearby radio galaxy Centaurus A. This lecture gives an account of the current state-of-the-art: After spelling out the scientific questions, the investigations of the dust tori in NGC 1068 and Circinus are used to demonstrate the observational challenge and the achieved data quality. The results of these studies provide new astrophysical insights and their comparison with newly developed models of dust tori allows a better understanding the identified structures. Finally, the prospects for extending this kind of studies to more distant and fainter AGN with current and next-generation VLTI instruments are discussed.

Key words:

Techniques: interferometric, Galaxies: active, Galaxies: individual (Circinus, NGC 1068, Centaurus A)

Contents

1	Introduction	1
1.1	Scientific questions to be addressed	2
1.2	Goals of this lecture	2
2	Observing active galaxies with MIDI	3
2.1	Instrumental setup of MIDI at the VLTI	3
2.2	Observational procedure	3
2.3	Observational results from MIDI	5
3	MIDI observations of the closest Seyfert 2 galaxies	6
3.1	The dust torus in the Circinus galaxy	6
3.2	The dust torus in NGC 1068	8
3.3	Summary: what did we learn so far about the tori?	9
4	Models of the gas and dust torus	9
4.1	Radiative transfer models	10
4.2	Hydro-dynamical simulations	11
5	The nucleus of the radio galaxy Centaurus A	13
6	Outlook: observations of fainter, more distant AGN	14
6.1	The AGN snapshot survey with MIDI	14
6.2	Exemplary results on distant AGN	14
6.3	The next steps	15
7	The future: new instruments at the VLTI	16
7.1	AGN studies with the near-infrared instruments AMBER and PRIMA	16
7.2	The second-generation mid-infrared instrument MATISSE	17
8	Summary	18

1. Introduction

There are several lines of indirect evidence, that in many Active Galactic Nuclei (AGN) the central engine – a super-massive black hole fed by a surrounding accretion disk – is embedded into an axi-symmetric, geometrically thick structure of gas and dust: the so-called torus (see lecture by Clive Tadhunter in this book). This dusty torus is held responsible for the observed dichotomy between Seyfert galaxies of type 1 and 2, respectively: in type 1, an unobscured view along the torus axis allows us to look directly into the central engine, while in type 2 objects the torus is seen edge-on and thus blocks our view towards the very center.

There are many different models for the geometry and density distribution of those tori in the literature (see lecture by Moshe Elitzur). They mostly try to explain the overall SEDs of Type 1 and type 2 AGN as well as their relative abundance by radiative transfer in disk- or torus-like dust distributions. However, as long as the dust emission of the structure remained unresolved, it was impossible to decide between these models.

In order to demonstrate the observational challenge in resolving these tori, I refer to a simple torus model (Schart-

Email address: meise@mpia.de (Klaus Meisenheimer).

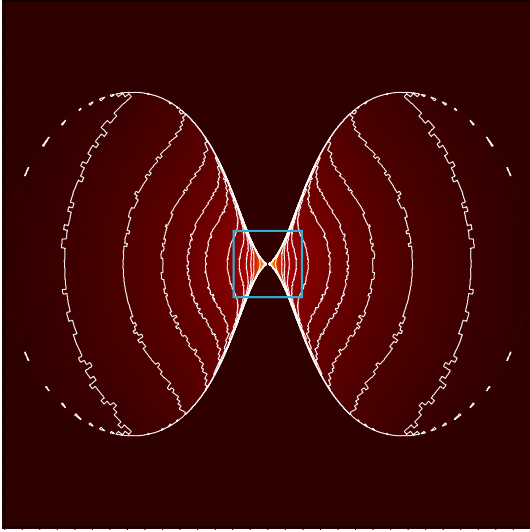


Fig. 1. Temperature distribution of a simple torus model (Schartmann et al., 2005). The dust temperature (logarithmic contours) ranges from > 1000 K in the innermost part to 80 K at the outer edge. A box depicts the region shown in Fig. 2.

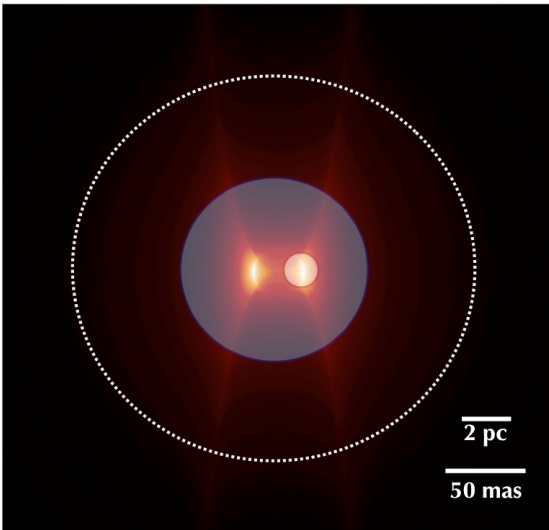


Fig. 2. Expected mid-infrared emission of the torus at a distance of 14 Mpc (*e.g.* NGC 1068, NGC 4151) compared to the angular resolution provided by different telescopes. On top of the central part of the torus model (Fig. 1), the beam width of a diffraction limited 8 m telescope operating at $10 \mu\text{m}$ (dotted circle) and $4.5 \mu\text{m}$ (grey shaded circle) is shown. The light shaded circle gives the beam width of a 100 m telescope at $10 \mu\text{m}$. Only a 100 m size telescope will be able to resolve sub-structures of the torus.

mann et al., 2005). Its basic geometry and temperature distribution are displayed in Fig. 1. Three-dimensional radiative transfer calculations predict SEDs and images at various wavelengths. In Fig. 2, the predicted image at $10 \mu\text{m}$ of such an *ideal* torus is used to demonstrate what one might resolve with various telescopes: a diffraction limited 8 m telescope at $\lambda = 4.5 \mu\text{m}$ (*e.g.* NACO at the VLT) will hardly resolve details of the torus emission even in the closest Seyfert galaxies. In order to resolve the structures at mid-infrared wavelengths around $10 \mu\text{m}$ a 100 m class telescope is required. In effect, this is what the MID-infrared

Interferometric instrument (MIDI; Leinert et al., 2003) at the VLT Interferometer (VLTI) provides, although in practice the aperture plane needs to be filled by a large number of two-baseline observations with various combinations of telescopes.

1.1. Scientific questions to be addressed

For the first time, the VLT Interferometer enables us to study the cores of nearby AGN with a linear resolution of $\lesssim 1$ pc. MIDI operates at $8 - 13 \mu\text{m}$, *i.e.* the wavelength range in which the emission of dust at temperatures $T \gtrsim 300$ K peaks. Thus, it is perfectly suited for investigations of the AGN heated dust distribution. The immediate aim of the MIDI observations of nearby AGN at mid-infrared wavelengths is to verify the torus paradigm by answering the following questions:

- Does a compact AGN heated dust structure – a “torus” – exist in the cores of AGN?
- What is the structure of the dust torus, *i.e.* what is its size and geometry, is it smooth or filamentary or clumpy? What is its temperature distribution?
- What is its orientation with respect to the source axis (as defined by radio jets and other outflow phenomena)?
- Do **all** AGN contain a dust torus?

It would be short-sighted to regard the torus merely as a light-blocking nuisance. It is rather the reservoir of gas which supplies the accretion disk with fuel. To understand the central fueling process, one would ideally witness directly how parts of the inner torus (possibly a turbulent disk as seen in the hydro-dynamical models, sect. 4.2) are caught by the black hole’s attraction and dragged towards the center. In nearby Seyfert galaxies this process should occur within radii $r < 1$ pc and on time-scales of years. Eventually investigations of the torus will try to answer

- the generic question: how are Active Nuclei fueled?
- And the more specific question: What role does the torus of gas and dust play in this?

1.2. Goals of this lecture

The *primary goal* of this lecture is to present the state-of-the-art of interferometric studies of AGN with MIDI at the VLTI. So far, the most extensive data sets have been obtained for two nearby Seyfert 2 galaxies – the Circinus galaxy and NGC 1068 (see Section 3). Some first results on the mid-infrared emission from the the nucleus of the nearest radio galaxy – Centaurus A are reported as well (Section 5). As observations with the two-beam instrument MIDI lack absolute phase information, they do not allow to reconstruct images directly. The data need to be interpreted by geometrical model fits. In order to understand these *observational* models in terms of the nuclear dust distribution it is necessary to confront the observations with the predictions of *physical* models. As *second topic*, therefore, I will present new theoretical simulations of dust tori,

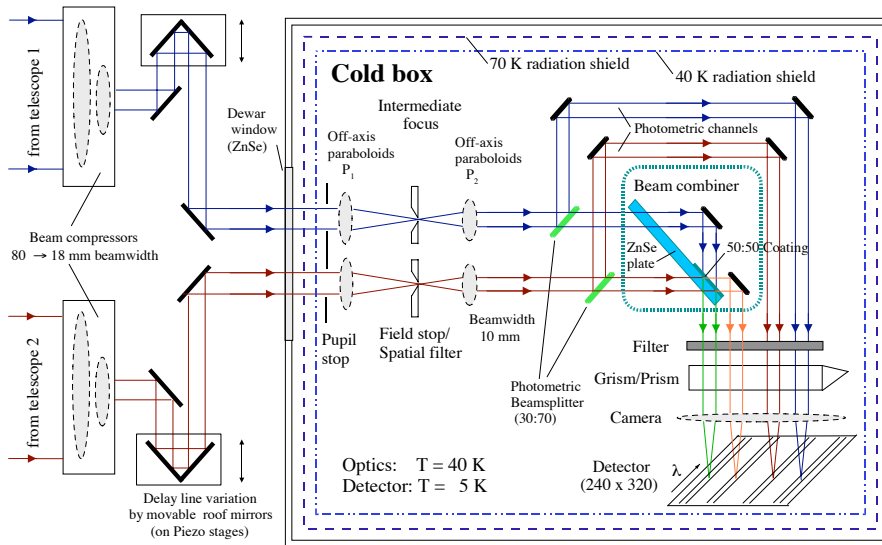


Fig. 3. Schematic diagram of MIDI. The beams from the two telescopes enter from the left and pass the “mini-delay-lines”, before entering the **cold box**. Here they are focused onto a slit (“spatial filter”) and re-collimated again. The beam combiner consists of a ZnSe plate which is partly coated with a layer transmitting/reflecting each 50% of the light and two folding mirrors. The two parallel photometric channels (light paths around the beam combiner) are not used in the *high-sensitivity mode* for faint targets.

and compare them with the MIDI observations. A *third goal* is to discuss the current limits of MIDI at the VLTI. To this end, observations of some very faint and distant AGN will be presented, and the immediate next steps will be outlined. *Finally*, the lecture will introduce the next generation of VLTI instruments and their promises for future AGN research.

2. Observing active galaxies with MIDI

2.1. Instrumental setup of MIDI at the VLTI

MIDI is a *two-beam* instrument (Fig. 3): it combines the light of only two telescopes at a time. For observations of AGN which typically have a flux in the N-band ($8 - 13 \mu\text{m}$) of $S_N \simeq 1 \text{ Jy}$ and below, the use of two 8 m *Unit Telescopes* (UTs) is mandatory to reach the required sensitivity. The light from the stationary Coudé-focus of each telescope is transferred in a tunnel to the “delay lines” (Fig. 4). The delay lines contain a system of movable mirrors which allow to compensate the light path difference between the beams of the telescopes before the light enters the interferometric laboratory. Here both beams are reflected into MIDI. The instrument consists of a “warm optics” that is needed to feed the light into the heart of the instrument and contains two “mini delay lines” which are able to modulate the path difference by a few millimeters (see schematic diagram in Fig. 3). The heart of MIDI is the *cold box* which measures only $90 \times 50 \times 40 \text{ cm}^3$ and is cooled to 40 Kelvin. It contains the “cold optics” and the detector (which itself is cooled to 5 Kelvin). The center of the cold optics is the

beam combiner that consists of a ZnSe plate¹ and is coated partly by a layer transmitting and reflecting each 50% of the light, plus two additional mirrors. In this way, two “interferometric beams” are formed. Note that the *pupils* of both telescopes are re-imaged onto the ZnSe plate: MIDI is a “pupil-plane interferometer”. The interferometric beams then pass a filter-wheel and a NaCl prism before being re-focused onto the detector. The prism disperses the light between 7.5 and $13.5 \mu\text{m}$ into a spectrum with a resolution of $R = \lambda/\Delta\lambda \simeq 30$. Alternatively, a grism ($R = 230$) can be introduced. Since the reflection at the coating introduces a phase shift by π , the *fringe patterns* (modulations due to constructive or destructive interference) have opposite sign in the two spectra – i.e. a maximum in one spectrum corresponds to a minimum in the other. Since the spectral range $\Delta\lambda = 6 \mu\text{m}$ is more than half the central wavelength often both a maximum and a minimum can be seen in both spectra.

2.2. Observational procedure

To carry out observations with a single VLT telescope is not a trivial matter: dozens of control mechanisms of the telescope and the instrument have to work together. So imagine to use two of them at the same time!² In fact, there

¹ Glass or quartz do not transmit $10 \mu\text{m}$ radiation. Thus special materials like ZnSe or NaCl (salt) have to be used for transmission optics. Whenever possible, reflective optics (mirrors) are used.

² It should be noted that in order to obtain a stable fringe signal on the MIDI detector around 400 CPUs in the VLTI and MIDI have to work side by side.

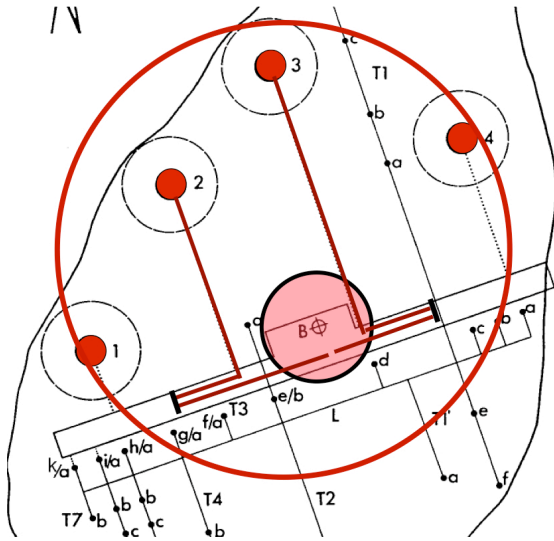


Fig. 4. Setup of the VLTI. The four UTs are distributed over an area of 125 m diameter (large circle). Here, for example, the light of UT2 and UT3 is fed into the tunnels which guide it to the delay lines (indicated by a single mirror). From there they reach the interferometric laboratory (small shaded circle). The delay mirrors are positioned such that the total path lengths of light from a distant source via UT2 equals that via UT3. In the laboratory the two beams are directed into MIDI. All together each beam undergoes 20 reflections before entering the warm optics of MIDI.

are already six steps to be taken, before the interferometric integration on a target can start:

- (1) Both telescopes have to point to the same source.
- (2) The main mirrors of the VLTI UTs possess an active support system which allows to optimize their shape. The active system has to be controlled by observing a guide star. At each telescope an appropriate offset guide star has to be targeted and the active mirror control has to be started.
- (3) The atmosphere distorts the wavefront of a source across the diameter of one single 8 m telescope. But only parallel patches of the two wavefronts can interfere. Thus an adaptive optics (AO) system in the Coudé focus of each telescope (MACAO) is needed to "straighten" the wavefront. Either the target or a star within $57''.5$ have to be fed into MACAO and its control loop has to be closed.
- (4) Anything at room temperature (~ 300 K; e.g. atmosphere, telescope, tunnels, dust on the mirrors) has its peak thermal emission around $12 \mu\text{m}$. Thus, in the N-band, the background is orders of magnitude larger than the signal from an AGN. In order to see the target on the detector one has to alter the pointing of the telescope rapidly (frequency: a few Hz) between the source position and a "blank sky" position some $10''$ off the source, and subtract the *on* and *off* signal in real time ("chopping"). This is done by wobbling the secondary mirrors M2 of both UTs. Even then faint sources can hardly be identified in the two acquisition images which show only a field-of-view of $2''$ diameter (Fig. 5). In addition, chopping makes life harder

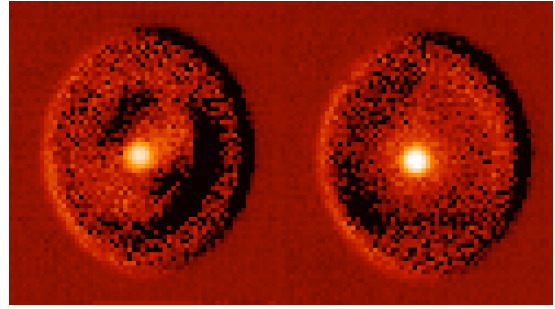


Fig. 5. Target acquisition in MIDI. The two images of a rather bright AGN (Circinus) are shown, which are delivered by telescopes 1 & 2 onto the MIDI detector. The field-of-view has $2''$ diameter. Note the uneven background structure, which is caused by imperfect cancelation of the on-target and off-target images during chopping of the M2s. This can severely hamper the detection of fainter sources.

for MACAO. So, under mediocre conditions it is not uncommon that the AO loop (3) breaks down again.

- (5) When the target is identified in both images, it has to be moved onto a certain position in order to send the light through the slits, which will be moved into the focal plane for the interferometric observations, and to secure optimum overlap between the two beams. This is done by a procedure which determines the actual position of the target and adjusts the telescope pointing accordingly.

In fact our experience with faint sources is that managing steps (3..5) is the hard bit of the MIDI observations. The interferometric part is comparably easy:

- (6) First MIDI is set up for interferometric observations: the slits and the prism are moved in. The chopping of the M2s is turned off. A "fringe search" changes the *optical path difference* (OPD) between both telescopes by moving one delay line by several millimeter, modulated by a rapid movement of one of the roof-mirrors (Fig. 3) in order to find the maximum fringe amplitude at $\text{OPD} = 0$.
- (7) After the the fringe is found, the *interferometric integration* is started, during which the OPD is stabilized on the fringe signal. It typically consists of several thousand frames of very short integration time ($\Delta t = 12$ or 18 ms DIT).
- (8) The interferometric observation has to be followed by a pair of *photometric integrations*: First, the beam of telescope 2 is blocked, and two photometric spectra of the source (the beam-combiner in Fig. 3 now serves as *beam-splitter*) through telescope 1 are recorded on exactly the same detector pixels as the interferometric spectra. Second, telescope 1 is blocked and spectra from telescope 2 are recorded. For the photometric observations the chopping of the M2s has to be turned on again.

Experience shows that one observational sequence (steps 1..8) takes a minimum of 20 minutes. For faint targets such as AGN (difficult steps 3 and 4; larger number of integrations) up to one hour is required.

For calibration of the photometric flux and the fringe amplitude a standard star of known spectrum and diameter has to be observed frequently with the same observational sequence (1...8). Thus, a fully calibrated MIDI observation with one projected baseline between two telescopes takes about one hour. In the following we will refer to such an observation as a *visibility point*.

2.3. Observational results from MIDI

The frames recorded by the MIDI detector have to be analysed by a special software package ("pipeline"). We use the "coherent" method of the EWS (Expert Work Station) pipeline written by Walter Jaffe (Jaffe, 2004), since it provides the most accurate results for faint sources. It is beyond the scope of the present article to explain details of the data reduction. So, the reader is referred to the articles by Olivier Chesneau (2007) and Konrad Tristram (2007) in the first volume of this series. Here, I only want to discuss the final, calibrated output of the data reduction:

Figure 6 displays the result of MIDI observations of a relatively faint target, Centaurus A (the scientific results will be discussed in Section 5) on February 28, 2005. Two complete measurements (interferometric and photometric integration on target and standard star), separated by two hours were obtained. The light within the MIDI range ($7.8 \lesssim \lambda \lesssim 13.2 \mu\text{m}$) has been dispersed by the prism ($R = \lambda/\Delta\lambda \simeq 30$). The *top panel* shows the result of the photometric measurements: they represent the *total flux* F_{tot} of Centaurus A within MIDI's slit (width: $0''.5$). F_{tot} is calculated from the (geometrical) average of the two photometric integrations obtained for telescopes 1 and 2, respectively (see step 8, above), and calibrated by a standard star observation. As expected they agree within the formal errors, although it is obvious from the scatter of the data around a smooth spectrum that the intrinsic (photon noise) error is somewhat smaller. This indicates that the discrepancy at longer wavelengths is introduced by a systematic effect. In the present example we identify it with the uncertainty in the subtraction of the background underneath the photometric spectra.³

The *middle panel* displays the spectra of the *correlated flux* F_{corr} derived from the fringe amplitude of the interferometric integrations. In this case the discrepancy is larger than the formal error and almost constant across the wavelength range. We regard the difference as a real effect: Centaurus A is slightly more extended in the baseline orientation along position angle P.A. = 119° than along P.A. = 96° , thus leading to a reduced fringe amplitude. Background subtraction is not an issue for the interferometric measurements since the background signal is uncorrelated and thus does not contribute to the fringe amplitude.

³ The chopping does not perfectly subtract the sky background on-line. Thus, a local background is determined next to the photometric spectra and subtracted in the data reduction.

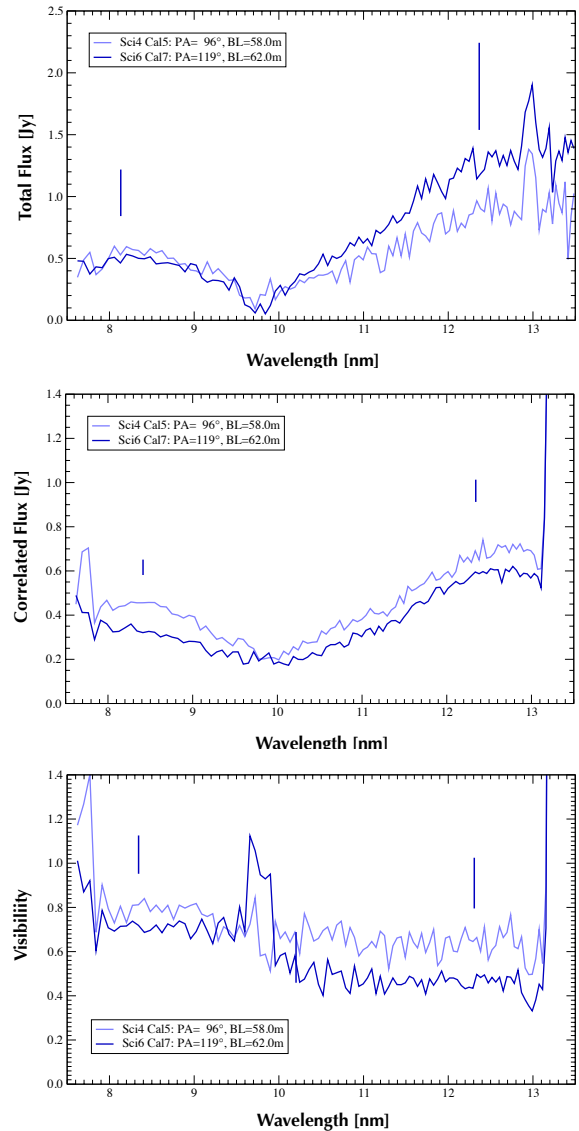


Fig. 6. Result of two MIDI observations of Centaurus A, separated by two hours (dark blue/black and light blue/grey lines). The *top panel* shows the spectrally dispersed *total flux* F_{tot} , the *middle panel* displays the *correlated flux* F_{corr} , and the *bottom panel* gives the resulting visibility $V(\lambda) \equiv F_{\text{corr}}(\lambda)/F_{\text{tot}}(\lambda)$. In each panel, typical formal errors are shown by vertical bars. The spectra of both F_{tot} and F_{corr} are dominated by a very broad absorption feature between 8.5 and $12 \mu\text{m}$ caused by silicate grains. Note that the SII emission line at $12.9 \mu\text{m}$ is only visible in the total flux within the entrance aperture ($0''.6$ diameter) but not in the interferometric spectrum ($0''.02$ resolution). The sharp feature at $9.7 \mu\text{m}$ in the visibility is caused by an imperfect calibration of the atmospheric ozone absorption in F_{tot} .

The visibility $V(\lambda)$ (*bottom panel*) is calculated in principle⁴ by $V(\lambda) = F_{\text{corr}}(\lambda)/F_{\text{tot}}(\lambda)$. The formal error of V is dominated by the error of F_{tot} . As one can see, the 15% difference in the correlated flux at $\lambda \simeq 12.5 \mu\text{m}$ is increased to 40% in V due to the division by F_{tot} . In addition, there is

⁴ The exact way depends on options set in the data reduction package.

a clear signature of an imperfect removal of the ozone band (around $9.75\ \mu\text{m}$) which can be identified with a depression seen in the total flux spectrum (top panel). Both effects indicate that in MIDI observations of *faint targets* one is not limited in accuracy by the interferometric measurement but by the uncertainties in the photometry. Therefore, it is preferable either to work with the correlated fluxes alone or use an average $\langle F_{\text{tot}} \rangle$ over all measurements in calculating V , when fitting the data by geometrical models. On the other hand, this approach is prohibited whenever any indication for an intrinsic variability of the source flux F_{tot} is present.

In the following the set of data $F_{\text{tot}}(\lambda)$, $F_{\text{corr}}(\lambda)$, $V(\lambda)$ is referred to as “one visibility point” although it contains about 20 independent measurements at various wavelengths (*i.e.* various positions in the Fourier plane $(U, V) = (X/\lambda, Y/\lambda)$, where X, Y are the projected baseline coordinates between both telescopes).

3. MIDI observations of the closest Seyfert 2 galaxies

3.1. The dust torus in the Circinus galaxy

The Circinus galaxy at a distance of 4 Mpc is the closest Seyfert galaxy. It shows all signs of a classical Seyfert 2: narrow allowed and forbidden emission lines, strong silicate absorption around $10\ \mu\text{m}$ and a heavily absorbed X-ray spectrum. An extended cone of emission line gas and the presence of broad lines in the polarized optical flux (caused by scattering) provide direct evidence that the central engine is hidden from our direct view behind a substantial amount of dust. Circinus is a spiral galaxy seen almost edge on. Thus, several magnitudes of extinction might be caused by the dust lanes in the spiral disk, behind which the nuclear region is located.

The highly southern declination of Circinus ($\delta = -65^\circ$) makes it an almost ideal target for the VLTI: it can be observed for up to 12 hours during long winter nights, thus allowing the projected baseline orientation between each two UTs to swing by up to 180° due to the earth’s rotation (see Fig. 7). In five observing runs during the MIDI *guaranteed time observation* program (Leinert, 2004) we have been able to collect 21 visibility points, most of them with the shortest VLTI baselines UT2–UT3 and UT3–UT4. They provide the most complete uv –coverage obtained for any extragalactic target so far. Already the six visibility points obtained with UT3–UT4 during one single night (Fig. 7) show two properties of the nuclear dust distribution (see Fig. 4 in Tristram, 2007): first, the structure is well resolved with a projected baseline $B \simeq 60\ \text{m}$ (angular resolution: $\Delta = \lambda/2B = 21\ \text{mas}$ at $\lambda = 12\ \mu\text{m}$) since $F_{\text{corr}}(12.5\ \mu\text{m}) < 1.5\ \text{Jy} \ll 13\ \text{Jy} = F_{\text{tot}}$. Second, the source is much more extended along P.A. = 45° than along P.A. = 135° ($F_{\text{corr}}(135^\circ) < 1/3 F_{\text{corr}}(45^\circ)$).

The lack of absolute phase information prohibits direct

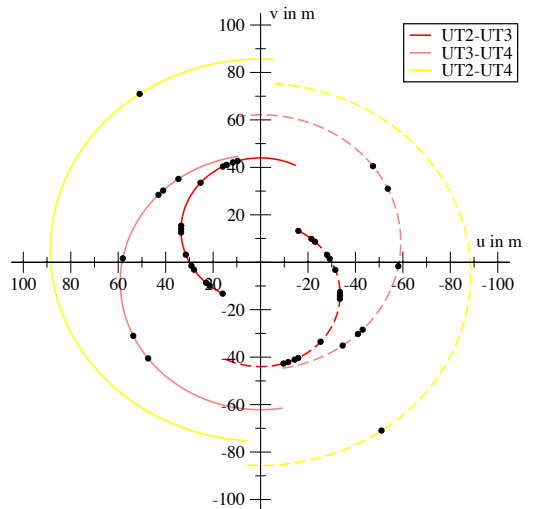


Fig. 7. Current coverage of the uv –plane with MIDI observations of the Circinus galaxy. The projected baseline is given by the distance between the origin and a point (symmetrical to origin as the telescopes are interchangeable). The dots show the observed visibility points for Circinus. The lines give the tracks through the uv –plane for the baselines UT2–UT3, UT3–UT4, UT2–UT4.

Table 1

Fit parameters of the image model for the dust torus in Circinus. At the distance of Circinus, 1 parsec corresponds to 50 mas.

Parameter	Component 1	Component 2
Major Axis a [mas]	21	97
Axis Ratio b/a	0.21	0.97
Total Silicate Depth $\tau_{9.7}$	1.2	2.2
Black-body Temperature [K]	334	298
Covering factor f	1.0	0.2
Position Angle (major axis)	61°	61°

image reconstruction from the MIDI visibilities. Instead we have to fit an *image model* to the observed spectra $F_{\text{corr}}(\lambda)$, using $F_{\text{tot}}(\lambda)$ as an additional constraint. It turns out that a minimum set of two components is required. We use two concentric elliptical Gaussian components for the spatial intensity distribution. The spectrum of each component is parameterized by a black-body spectrum of a certain temperature, modified by a foreground screen of dust absorption. The absorption coefficient is dominated by the broad silicate feature between 8.5 and $12\ \mu\text{m}$. A covering factor f allows for the possibility that the model surface is not smoothly filled with dust at the nominal temperature but encompasses also cooler (fainter) patches. The two-component image model is Fourier-transformed. A χ^2 fit to the observed $F_{\text{corr}}(\lambda)$ in the Fourier-plane determines the model parameters given in Tab. 1.

A schematic representation of the best fit model is shown Fig. 8: the very compact, elongated dust component 1 has only 0.4 pc diameter and may well represent a disk-like

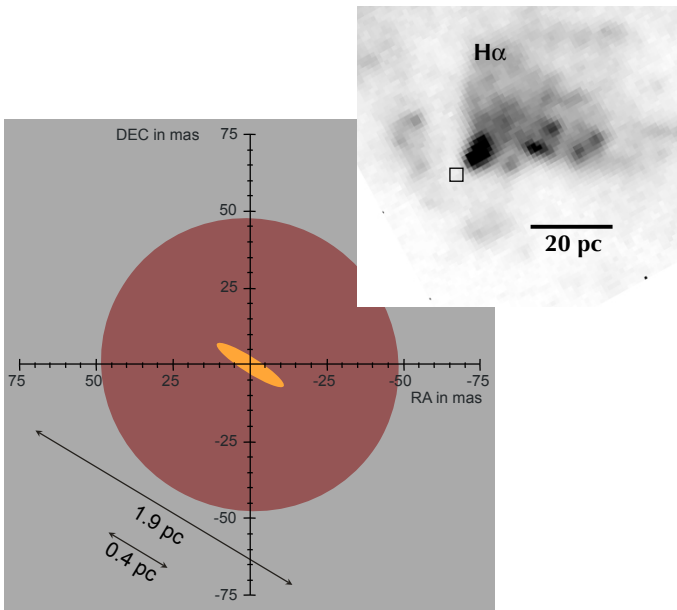


Fig. 8. Schematic representation of the image model of the dust distribution in Circinus (scale: 50 mas/pc). The Gaussian brightness distributions are represented by their size at half the maximum intensity. The insert shows the ionization cone as observed in $H\alpha$ (from Wilson et al., 2000). The small box represents the area of the main graph.

structure seen almost edge-on. It seems to be embedded in the much larger almost round component 2, which we identify with the “dust torus”. The low covering factor of the latter indicates that its structure is inhomogeneous and may consist of clumps or filaments with a wide range of temperatures $T < 300$ K. The emission of the inner disk formally suffers less silicate absorption than the torus. We interpret this as sign of silicate *emission* and therefore regard the formal value of its black-body temperature with great caution. An orientation of the dust structure can only be derived for the well-elongated disk: indeed the position angle of its axis (P.A. = -30°) is well consistent with the symmetry axis of the extended emission line cone (insert in Fig. 8). However, such a thin disk can hardly account for the confinement of ionizing radiation into a cone of $\lesssim 85^\circ$. Instead the extended torus component must contain a funnel along the axis which our current observations fail to detect due to their lack of dynamic range and coverage of the inner part of the uv -plane (but see discussion below).

The only study of the Circinus nucleus with comparable angular resolution are water maser observations with the southern VLBI (Fig. 9; Greenhill et al., 2003). They show a regular pattern of red- and blue-shifted maser spots, which the authors interpret by a Keplerian rotating disk of ~ 40 mas (0.8 pc) diameter. As the orientation of the maser disk is exactly parallel to that of the dust disk it seems sensible to identify both disks with each other (Fig. 9): although the maser spots straddle beyond the “effective size” of the dust disk (= FWHM of Gaussian intensity distribu-

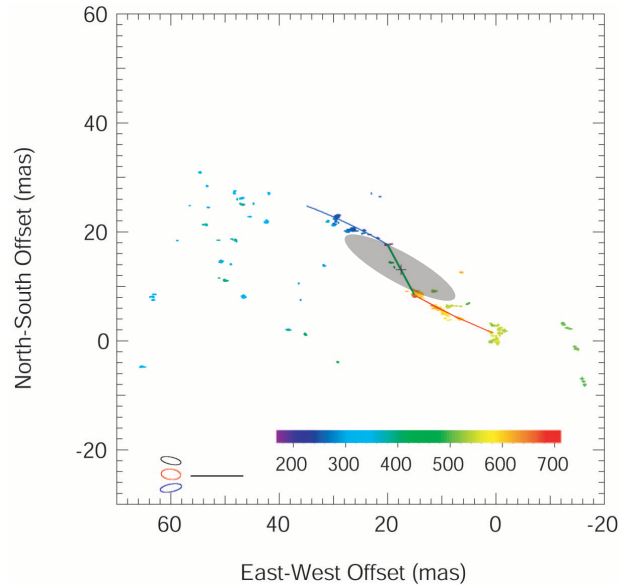


Fig. 9. Apparent position and radial velocity of the H_2O masers in Circinus (from Greenhill et al., 2003). The inner masers show Kepler rotation in a warped disk of 40 mas diameter. The dust disk (grey) seems perfectly aligned with the maser disk.

tion⁵), maser and dust disk may well be co-spatial. This would imply that also the dust disk is shaped by rotation around the super-massive black hole in the center of the Circinus galaxy.

Finally, the low covering factor $f = 0.2$ of the extended component is worth a more detailed investigation. Formally, it implies that only 20% of the surface of the torus component 2 are at the black-body temperature $T \simeq 300$ K, while most of it has lower emissivity due to lower temperature. As Moshe Elitzur pointed out in his lecture and as the section 4 on torus models will further discuss, we do not expect the torus emission to be smooth and “iso-thermal”, but rather “clumpy” or filamentary, exhibiting a wide range of temperatures. Indeed, this is supported by the details of our interferometric measurements with MIDI (see Fig. 10): the deviation of the measured values of the correlated flux from the prediction of a smooth model exceeds 7σ in several cases (upper row in fig. 10)! But the deviations do not look like random scatter – rather it seems that the data “wobble around” the smooth model. We investigated whether the wiggles are consistent with a patchy structure of the dust distribution (Tristram et al., 2007). To this end, a screen with randomly distributed transmission is put in front of the smooth model. About a thousand screens were realized, the resulting images were Fourier-transformed and fitted to the observed $F_{\text{corr}}(\lambda)$ searching for an improvement of the χ^2 value. As one can see in the lower panels of Fig. 10, the best-fit patchy model is able to reproduce the observed wiggles at least qualitatively.

Interestingly enough the random model which seems to fit the wiggles best, is one with a pronounced brightness

⁵ Note that the total size could be substantially larger.

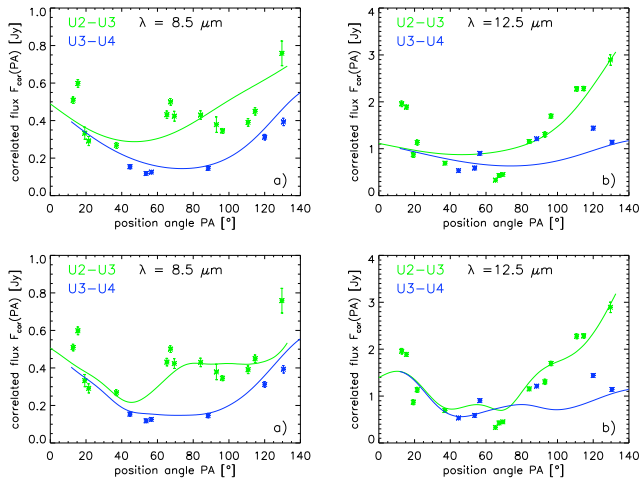


Fig. 10. Model fits to the correlated flux obtained with two different telescope combinations (as function of baseline orientation). *Upper row*: best fit for the smooth two-component model (Table 1). *Lower row*: fit to a random realization of a patchy distribution, generated by a foreground screen of varying transmission.

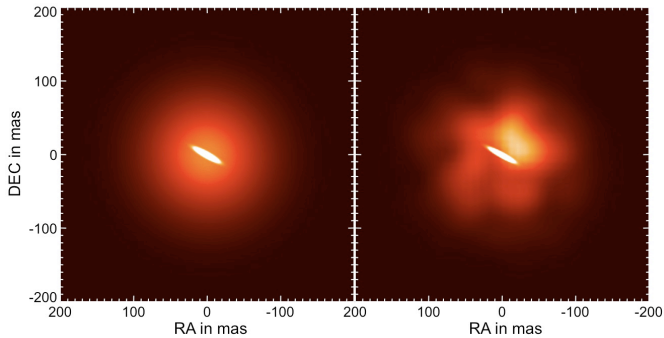


Fig. 11. Model images of the dust distribution in Circinus. *Left panel*: smooth model consisting of two concentric Gaussian brightness distributions. *Right panel*: patchy model as generated by modifying the Gaussian model with a foreground screen of randomly varying transmission.

peak on the putative *torus axis* (c.f. Fig. 8). Although the images have a 180° ambiguity, it seems obvious that an additional bright patch located roughly on the torus axis can substantially improve the fit. This can be regarded as first hint that MIDI “sees” some hot clumps or filaments along the funnel of the torus.

3.2. The dust torus in NGC 1068

The second AGN, for which detailed interferometric measurements have been obtained with MIDI, is the prototypical Seyfert 2 galaxy NGC 1068. It is the brightest extragalactic N-band source in the southern sky. At its distance of 14.4 Mpc, the scale is 14 mas/pc, *i.e.* structures of about one parsec can just be resolved with MIDI at the VLTI.

The earliest MIDI observations of NGC 1068 were obtained already half a year after MIDI became operational, during *Science Verification Time* (SDT). On their basis, Jaffe et al. (2004) could demonstrate for the first time that a

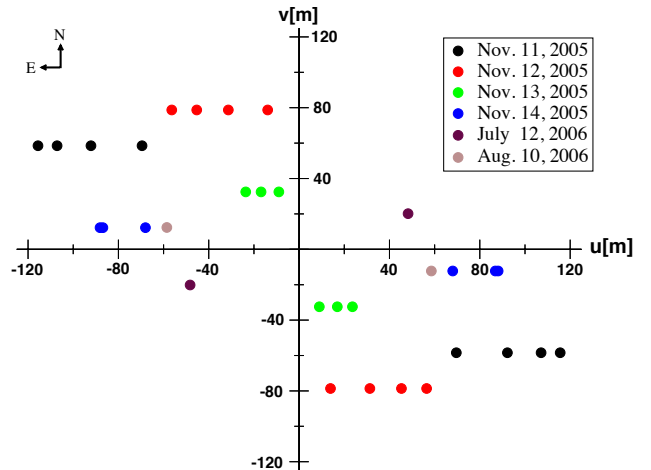


Fig. 12. Current coverage of the uv -plane by the MIDI observations of NGC 1068. Note the straight tracks which are caused by the equatorial position of NGC 1068.

compact, geometrically thick dust structure – as expected for the dust torus – indeed exists in Seyfert 2 galaxies. Essentially only two visibility points, one with UT2–UT3 and one with UT3–UT4, were observed. The observed correlated flux was best modeled by two components, a small, relative hot one ($T > 800$ K, diameter about 1 pc), embedded into a larger component of 320 K and about 3.5 pc diameter. With only two uv -points at hand, it was not possible to determine the shape and orientation *ab initio*. Under the assumption that the dust distribution is axi-symmetric to the radio axis, a slight East-West elongation was found for the extended component.

New observations with MIDI (Raban et al., 2008) cover the uv -plane much better (Fig. 12). To study the details of the silicate absorption profile with higher spectral resolution, the grism ($R \simeq 230$) was used for the new observations. As in the case of Circinus, a model of two components with Gaussian brightness distribution and blackbody spectrum describes the correlated flux data reasonably well. Due to the inclusion of the longest VLTI baselines UT1–UT3 and UT1–UT4, the measurements perfectly constrain the size, shape and orientation of the hot, inner component of the dust torus: its major axis measures 20 mas (1.4 pc FWHM), oriented along P.A. = 138° . It is rather elongated $b/a = 0.25$, not unlike the disk-shape structure in the Circinus nucleus. Only a lower limit, $T > 800$ K, can be set to the temperature. The lack of short baselines, < 50 m in the East-West direction (along u , see Fig. 12) makes the determination of the overall size and shape of the more extended “torus component” very uncertain: we regard its North-South extent of 56 mas (4 pc, FWHM) as a robust measurement, but the the East-West extent (42 mas = 3 pc) will need to be confirmed by shorter baselines along

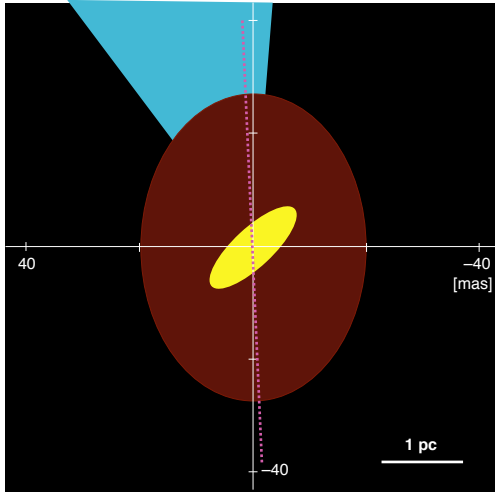


Fig. 13. Model image of the dust distribution in NGC 1068 derived from the MIDI observations. A hot inner component ($T > 800$ K) is embedded in a larger component of $T \simeq 300$ K. The orientation of the ionization cone and the radio axis (dotted line) are indicated.

East-West.⁶

The most intriguing fact about the inner, disk-like structure is that its symmetry axis at P.A. = 48° is neither aligned with the axis of the inner radio jet (P.A. $\simeq 2^\circ$) nor with that of the extended emission line cone (P.A. $\lesssim 20^\circ$). However, before speculating about the cause of this apparent misalignment, it is instructive to compare the dusty disk with radio observations of NGC 1068 at similar angular resolution: The overlay in Fig. 14 reveals that the hot inner component – as in the case of Circinus – is perfectly aligned with the spur of water masers extending towards the North-West from the nucleus. On the other hand, the minor axis of an apparent thick disk of radio continuum emission (presumably due to thermal bremsstrahlung of ionized gas), at P.A. $\simeq 15^\circ$ does much better align with the large scale ionization cone. This is an unsolved puzzle: is it possible that the inner part of the torus is misaligned both to the outer torus structure which confines the UV-radiation into the ionization cone *and* to the innermost, ionized gas distribution? Contrary to the interpretation of the hot elongated component as tilted circum-nuclear dust disk (Raban et al., 2008), I would rather propose to interpret it as dense filament which might extend asymmetrically from the core (note that we have no information how to place the hot dust component onto the radio maps in Fig. 14). This possibility is also favored by the fact that the water masers do not show the regular velocity pattern which would be expected for a rotating disk (as present in the Circinus galaxy).

⁶ Such baselines are provided by the Auxiliary Telescopes (ATs). A MIDI observation program with ATs is under way and has detected fringes from NGC 1068 already.

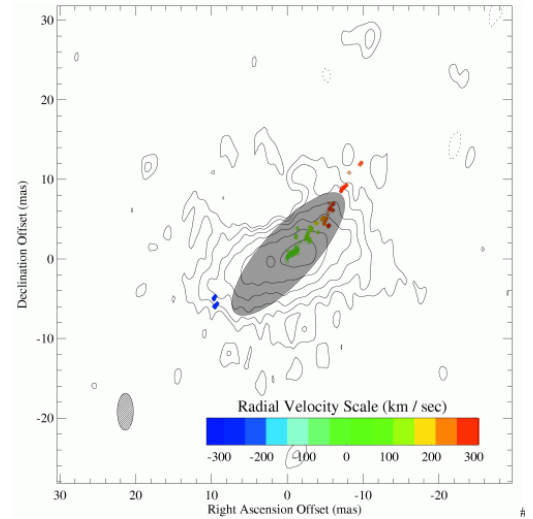


Fig. 14. Relative orientation of the hot dust component (grey shaded ellipse) and the radio sources in the nucleus of NGC 1068: radio continuum emission at 5 GHz (contours) and water maser (colored spots, from Gallimore et al., 2004). Note that the relative positions of radio map and dust component are unknown.

3.3. Summary: what did we learn so far about the tori ?

Let me summarize the generic results of the interferometric observations of the two brightest, nearby Seyfert 2 galaxies with MIDI in a few points:

- AGN heated dust structures do exist in Seyfert 2 galaxies. This supports the basic idea of the *unified scheme* that a geometrically thick dust structure absorbs the UV-optical radiation towards our line of sight. From the extinction towards the radiating surface of the extended components in Circinus and NGC 1068 (based on the optical depth in the silicate feature) we infer that about half of the total dust column density toward the AGN core is located inside the inner few parsecs.
- The most intense dust emission is emitted by rather small very elongated structures which might represent a disk-like component seen almost edge-on. This structure is aligned (co-spatial?) with the location of water masers. In Circinus there is substantial evidence for a rotating disk, while the situation in NGC 1068 remains unclear as the orientation of the elongated structure does not fit to the source axis. As Circinus and NGC 1068 also differ in other aspects, there does not seem to exist such a thing as a “standard torus”.
- The three-dimensional structure of the extended dust components remains unclear, since the observational model of a Gaussian brightness distribution smoothes out any information beyond the mere size and overall shape.
- If the inner dust structures are geometrically thin disks, they can hardly provide the confinement of the ionizing radiation. Thus, the confinement has to occur further out, on scales $\gtrsim 1$ pc.

4. Models of the gas and dust torus

As we saw in the previous section, even the most extensive studies of nearby AGN with MIDI have collected only 15 to 20 visibility points. The correlated flux (or visibilities) are fitted by smooth models composed of simple components. Both common sense and astrophysical considerations (see *e.g.* Krolik and Begelman, 1988, and lecture by Moshe Elitzur) tell us, however, that in reality such smooth distributions cannot exist and have to break down into individual clouds or clumps or filaments. Therefore, well before the first MIDI observations were obtained, a complementary, theoretical study was triggered with the aim to understand how tori could form and how they would radiate in the mid-infrared. Starting from radiative transfer calculations of simple, analytic torus models, we worked our way through a detailed study of a torus which is composed of a large number of randomly distributed clouds (Schartmann et al., 2008a). Currently we are undertaking the first steps towards a *physical* model of the gas and dust distribution in the nuclei of galaxies: employing hydro-dynamical simulations we try to understand which kind of cool, dense gas structures would naturally form and survive in the central parsecs around the AGN core (Schartmann, 2007).

4.1. Radiative transfer models

As we have seen in Section 3 the current state of infrared interferometry falls still some way short of delivering *true* images. All we can do at the moment is to take an image model, Fourier-transform it and compare it with the observed correlated fluxes (or visibilities). We started from the simplest, well-behaved models: a sum of several Gaussian brightness distributions of dust emission at a certain temperature. For instance, the expected temperature gradient between hot dust close to the accretion disk and the outer more distant parts of the torus can only be approximated in this model by a hotter inner and cooler outer component (such as the components in NGC 1068). Also the Gaussian components might not have any obvious equivalent in the real world, although the inner “disks” in Circinus and NGC 1068 could well correspond to physical disks or rings of gas and dust (see discussion in 4.2, below).

An alternative approach is to start from a physical model (*i.e.* a given density distribution around the central engine), illuminate it with the radiation of the accretion disk, and predict the emerging images at various wavelengths. These images can then be compared with the observations in the same fashion as the simple image models. The dust emission which we observe in the mid-infrared is radiated from dust grains which are heated by the optical–UV–X-ray spectrum from the core. The emitted photons can heat other dust grains. Also they will be scattered and therefore diffuse on random walks through the dust distribution. *Radiative Transfer* (RT) calculations try to follow all these processes, to calculate the resulting temperature dis-

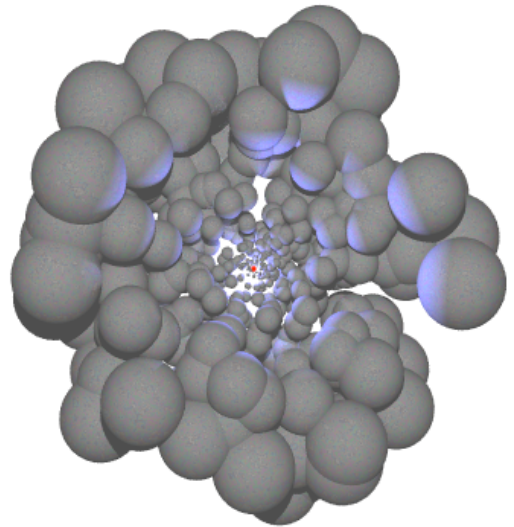


Fig. 15. Structure of a clumpy torus composed of spherical clouds, the size of which increases with radius.

tributions and finally to deliver images and spectra of the emerging radiation at various wavelengths.

Our RT calculations of various torus models (Schartmann et al., 2005, 2008a) employ the Monte Carlo Code MC3D (Wolf, 2001), which is able to track photon packages through any given density distribution in a 3-dimensional grid. The underlying physical model for the torus structure is the *Turbulent Torus Model* (TTM; Camenzind, 1995): it assumes the gravitational potential of a central black hole and a compact nuclear star cluster (core radius several tens of pc, depending on the black hole mass). Gas and dust is injected into the system by the mass loss from the stars (winds of asymptotic giant branch stars and planetary nebulae). Thus the gas shares the random motions of the hot stellar system. In addition, a rotational velocity of about 100 km s^{-1} is assumed. This leads to an “angular momentum barrier” close to the center. The resulting, effective potential has a shallow minimum at a radius of several parsec and confines the gas and dust (clouds) in a torus-shaped structure (see Fig. 1).

First, we calculated the RT through a continuous dust distribution (Schartmann et al., 2005). This is a sensible approximation if the clouds are very small compared to the total torus extent and sufficiently densely packed that the mean free path between each two clouds is not much larger than the cloud size. Mid-infrared images of such a continuous model are dominated by the emission from the inner wall of the funnel (*c.f.* right panel in Fig. 17). In the edge-on view (Seyfert 2) the image, therefore, would appear more extended *along* the torus axis.

However – as mentioned before – the gas and dust distribution in the torus is expected to be highly discontinuous. In his lecture Moshe Elitzur presents RT calculations for a such a discontinuous dust distribution which consists of hundreds of identical clumps.

We follow a slightly different approach: our clumpy torus is composed of randomly distributed spherical clouds, the

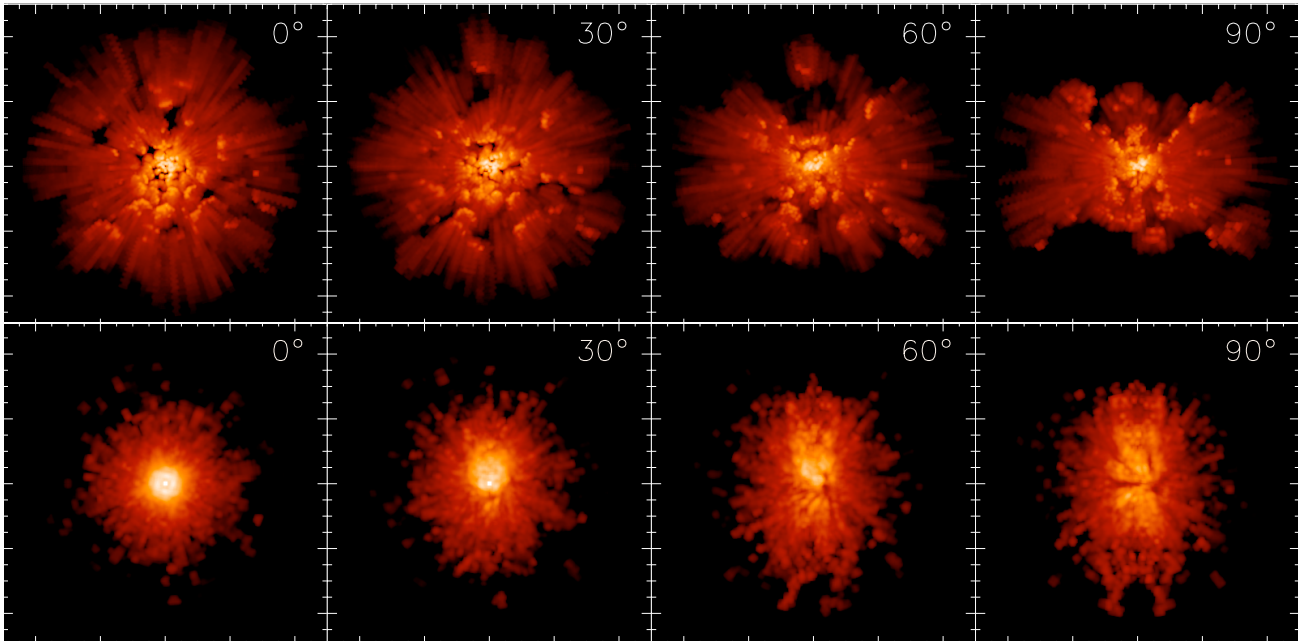


Fig. 16. *Upper row*: Mid-infrared images of the clumpy torus model at $\lambda = 12 \mu\text{m}$. *Lower row*: Mid-infrared images of the hydro-dynamical torus model at $\lambda = 12 \mu\text{m}$. The size of each panel is $100 \text{ pc} \times 100 \text{ pc}$.

size of which increases with distance from the AGN core (Fig. 15). Nevertheless, we keep the optical depth through each cloud constant, that is the gas and dust density is decreasing outwards. For computational reasons we had to choose a wedge-like geometry for the torus. The average density distribution (per unit volume) follows a powerlaw, which is also used in a continuous comparison model with the same wedge-like geometry. We perform a wide parameter study, in which the size distribution of the clouds, their filling factor, and their total dust mass are varied in order to investigate their influence on the emerging spectra and images (for details see Schartmann et al., 2008a). Our main goal was to understand how the broad silicate feature between ~ 9 and $12 \mu\text{m}$ (*c.f.* Fig. 6) is influenced by the cloud size distribution and total dust mass in the torus. In addition, we aimed to see whether the clumpy structure leaves any observable imprint on interferometric measurements with MIDI. To this end also images at various wavelengths were generated. The upper row of Fig. 16 shows mid-infrared images of the clumpy torus as they would be seen at different inclination angles between face-on ($i = 0^\circ$) and edge-on ($i = 90^\circ$). It is obvious that the radiation from hot dust is not confined to the innermost parts of the cloud distribution but also arises in distant clouds which “see” the accretion disk through free lines-of-sight in between the clouds. Likewise, some hot dust surfaces are hidden behind cooler dust clouds on our line-of-sight. As a combined effect, the silicate feature becomes less pronounced than in a continuous torus model: emission in the silicate line is suppressed in the face-on view (Seyfert 1) while in the edge-on view (Seyfert 2) the deep absorption trough is partly filled by emission. We demonstrate that the emerging mid-infrared spectra of both types perfectly match the observed

range of spectra from Seyfert galaxies (Schartmann et al., 2008a).

The comparison between the clumpy and the continuous torus in Fig. 17 demonstrates the enormous difference in apparent morphology: the very regular and symmetrical structure of the continuous model – essentially the inner walls of the axial funnel – is completely dispersed in the clumpy model. Individual, randomly distributed clouds in the vicinity of the radiation source dominate the emission. So neither a disk- or ring-like feature (as it is apparent in the continuous model) would appear. High-frequency variations of the visibility throughout the uv -plane (as observed in Circinus, *c.f.* Fig. 10) are predicted, and in fact can explain the wiggles in the Circinus data (*c.f.* Fig. 10). In addition, one expects rather large (random) asymmetries which might be detectable in the relative phase between $8 \mu\text{m}$ (hotter dust) and $13 \mu\text{m}$ (cooler dust). Also asymmetries between the illuminating point source and the dust structures might be detectable.

4.2. Hydro-dynamical simulations

So far, all torus models in the literature are based on pre-defined density distributions from which spectra and images have been calculated using various RT codes. In the course of these studies, continuous density distributions have evolved from simple disk- or wedge-shaped geometries to physically motivated distributions (like the TTM discussed in 4.1, above). Also the clumpy models (see *e.g.* Elitzur, these proceedings, and Hönig et al., 2006) start from an analytical cloud distribution which tries to reproduce some astrophysically motivated properties of the circum-nuclear gas and dust distribution. But a self-

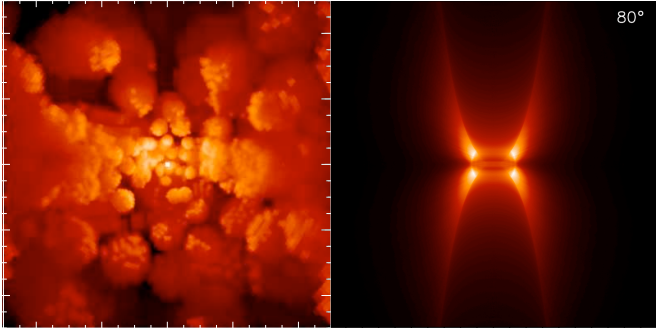


Fig. 17. Comparison of the central region of a clumpy (*left*) and a continuous torus model (*right*). The panel size is $20 \text{ pc} \times 20 \text{ pc}$. For the less luminous Seyfert 2 galaxies NGC 1068 and Circinus, we expect structures which are $2 - 5 \times$ smaller.

consistent astrophysical model needs to take into account the origin of the gas, its velocity distribution, cloud-cloud interactions, heating and cooling of the gas etc. Thus a 3-dimensional hydro-dynamical simulation of the central gas distribution in the galactic nucleus is required.

Our hydro-dynamical model (Schartmann et al., 2008b; Schartmann, 2007) starts from the basic assumptions already underlying the TTM (Camenzind, 1995):

- (1) The center of the Seyfert galaxy hosts a young stellar cluster.⁷ It needs to be of intermediate age (40 to 100 Myr) in order to make sure that stars with $M > 8 M_{\odot}$ have already reached the end of their life cycle, since their violent type II supernovae (SNe) explosions would blow away any gas and dust. The star cluster is dynamically supported by a random velocity dispersion and rotates slowly. Indeed, Ric Davis shows in his contribution to this book that most nearby Seyfert galaxies host such kind of intermediate age star clusters.
- (2) The nuclear star cluster is a source of gas (and dust) from stellar mass loss during the AGB phase and from planetary nebulae. The ejected gas shells initially carry the velocity of their parent stars. After about 40 Myr SNe Ia (arising in close binaries) become frequent and inject thermal and kinetic energy into the system.
- (3) Gas clouds collide and are stirred up by the SN explosions. In over-dense regions cooling occurs and leads to a runaway process (cooling instability) which produces cool, dense regions.
- (4) At present, our simulations use a serial code (TRAMP, Klahr et al., 1999). A reasonable time span can only be reached by splitting the computational domain in three “onion shells”. We start with the outer region, which set the boundary conditions for the middle zone, and so on.
- (5) The simulations start at 40 Myr after the formation of the stellar cluster and run for a short period (10

⁷ The existence of a young star cluster implies that a violent burst of star formation happened several ten million years ago in the central region.

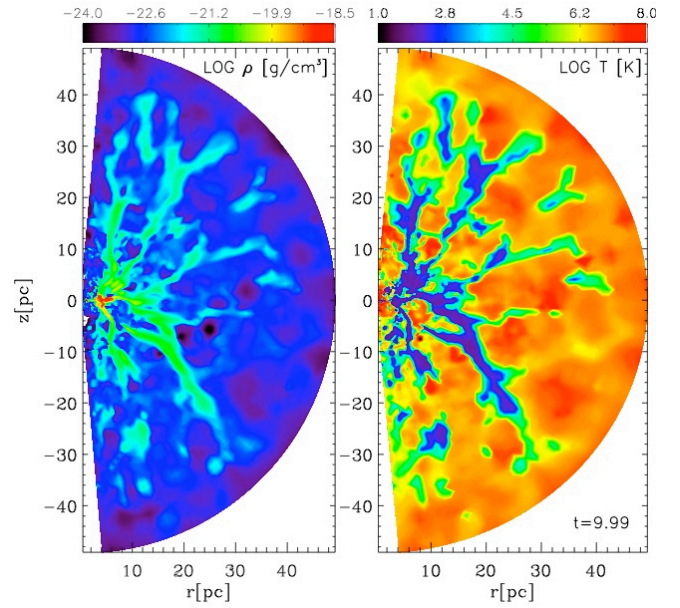


Fig. 18. Meridional cuts through the hydro-dynamical torus model for density (*left panel*) and temperature (*right panel*), respectively. Note that because cooling efficiency $\propto n^2$, the regions of highest densities show the lowest temperatures.

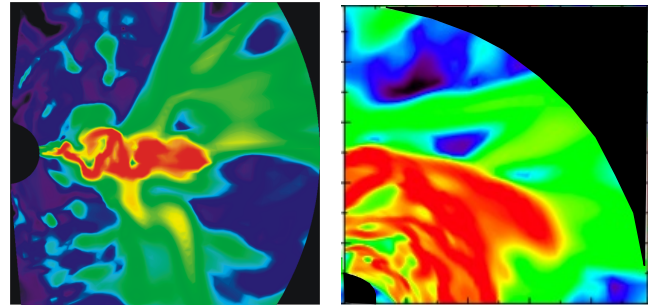


Fig. 19. Density distribution in the innermost 10 pc of the hydro-dynamical torus model. *Left panel*: meridional cut, *i.e.* the innermost part of Fig. 18. *Right panel*: equatorial cut through one quadrant. Near the momentum barrier at $r \simeq 3 \text{ pc}$ a very turbulent disk of high gas (and dust) density forms.

orbits at $r = 5 \text{ pc}$, *i.e.* 1.2 Myr) due to computational limitations. A quasi steady state is reached after one orbit already. Standard values for the mass injection and supernova rate of a 40 Myr old stellar population are taken from the literature.

Under these assumptions (and with our current limits in spatial resolution) a very interesting gas structure develops (Fig. 18):

- The densest (and hence) coolest gas forms filaments which extend radially (due to the radially out-flowing super-wind from the SN explosions).
- Close to the angular momentum barrier (around $r = 3 \text{ pc}$ in our model) a very dense, turbulent disk develops (Fig. 19). It accumulates the gas flowing inwards along the cooling filaments. Since no realistic viscosity is implemented in our current simulations, the angular momentum transport in the turbulent disk cannot be modeled correctly and the flow towards the black hole (which

would drain the disk at its inner boundary) cannot be followed.

In summary, the simulations predict that the gas torus in AGN essentially is composed of three constituents: dense radial *filaments*, a very dense *turbulent disk*, and large *voids*, which are filled with very hot gas ($T > 10^6$ K).

Already the density distribution (left panel in Fig. 18) has a global resemblance with our MIDI results of the Circinus galaxy: The observed, patchy torus component would then consist of filaments. A better way to visualize the mid-infrared emission of the hydro-dynamical torus model is to use the simulated density distribution as input for the RT calculations. Regions with $T < 1000$ K are populated with dust according to a constant gas-to-dust ratio and illuminated by the radiation of the accretion disk. The resulting $12\ \mu\text{m}$ images are displayed in the lower row of Fig. 16. The radial structure of filaments is clearly evident in the mid-infrared images. However, the dense disk does not appear as bright feature but rather leads to a shadowing effect since its very high density causes several magnitudes of extinction even at $\lambda = 12\ \mu\text{m}$. In this respect, the hydro-dynamical model seems in conflict with the observations.

5. The nucleus of the radio galaxy Centaurus A

The radio galaxy Centaurus A (= NGC 5128) plays a key role in extragalactic astronomy: at a distance of only 3.8 Mpc it is the closest large *elliptical galaxy*, the closest *galaxy merger* and the closest violent AGN. At its distance 1 pc corresponds to 53 mas. The kinematics of a parsec-scale disk of molecular gas allowed Håring-Neumayer et al. (2006) to derive an accurate mass of the super-massive black hole in its center: $M_{\text{bh}} = 6 \times 10^7 M_{\odot}$. The radio source has been observed over seven orders of magnitude in angular scales, from the VLBI jets (a few mas) to the outer lobes (several degrees). Extinction in the dust lane of the merging spiral galaxy severely obscures our view towards the nucleus of Centaurus A. Thus observations at infrared wavelengths are mandatory (see Meisenheimer et al., 2007, and references therein for more details).

Centaurus A was observed in early 2005 with MIDI using two telescope combinations: UT3–UT4 (on February 28) and UT2–UT3 (May 26). In both nights two visibility points were obtained, separated by about two hours. The projected baseline on February 28 was orientated roughly perpendicular to the parsec scale radio jet, while on May 26 it was aligned with it (Meisenheimer et al., 2007). We found that the mid-infrared emission is marginally resolved perpendicular to the jet axis with a 60 m projected baseline ($V \simeq 0.6$, *c.f.* Fig. 6), whereas it remains unresolved along the jet axis (projected baseline $\simeq 45$ m). Accordingly, we conclude that the 8 to $13\ \mu\text{m}$ emission from the core of Centaurus A is dominated by an unresolved point source (FWHM < 6 mas), which contributes between 50 and 80% of the total flux at $\lambda = 13\ \mu\text{m}$ and $\lambda = 8\ \mu\text{m}$, respectively. The extended component is tiny (FWHM $\simeq 30$ mas), as

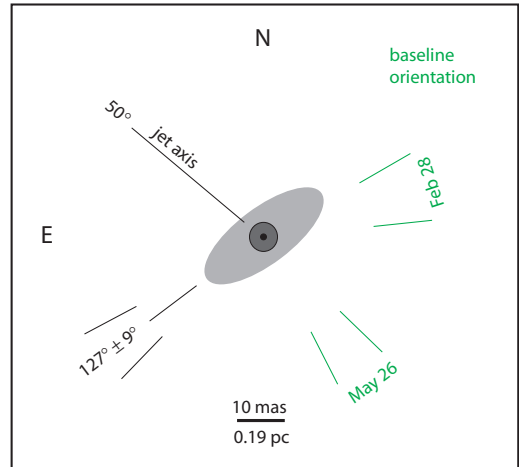


Fig. 20. Sketch of the mid-infrared emission from the inner parsec of Centaurus A. We identify the unresolved point source of < 6 mas FWHM (dark grey) with the VLBI core (FWHM = 0.5 ± 0.1 mas, indicated as black dot). It is surrounded by an elongated structure of dust emission (light grey) the major axis of which is oriented along $P.A. = 127^\circ \pm 9^\circ$ as inferred from the orthogonal baselines observed on May 26. From the visibilities observed with two baselines on February 28 we derive a major axis length of about 30 mas. Note that the major axis orientation is consistent with being perpendicular to the radio jet axis, and the axis ratio could be explained by a thin disk, the axis of which is inclined by $\sim 70^\circ$ with respect to our line-of-sight.

well, and seems elongated perpendicular to the radio axis (see sketch in Fig. 20). However, a better uv -coverage (including longer baselines) will be required to constrain the size, shape and orientation of this extended component more accurately. We interpret the extended component as dust emission from a small disk (diameter $\simeq 0.6$ pc).

We identify the unresolved component with the non-thermal “synchrotron core” of Centaurus A, since we find that – after correcting for the foreground extinction of $A_V = 14$ mag (derived from the depth of the silicate absorption) – its flux level and spectrum lies perfectly on the extrapolation of the power-law spectrum observed at millimeter wavelengths (Fig. 21). Together with spatially well-resolved photometry at shorter wavelengths (from HST and the AO camera NACO at the VLTI) we conclude that the unresolved point source fits perfectly to a canonical synchrotron spectrum. The spectrum is characterized by a rather flat power-law $F_\nu \propto \nu^{-0.36}$, cutting off exponentially at a cut-off frequency $\nu_c = 8 \times 10^{13}$ Hz. Below $\nu_1 = 4.5 \times 10^{10}$ Hz it becomes self-absorbed. We interpret this “synchrotron core” as the base of the radio jet (for details see Meisenheimer et al., 2007). Assuming that its size is only 0.5 mas (0.01 pc) as determined by radio VLBI observations at 43 GHz (Kellermann et al., 1997), and regarding the γ -ray spectrum at energies > 100 keV as *synchrotron-self-Compton* radiation, we find a self-consistent description for the synchrotron core which implies at most moderate Doppler boosting (Doppler factor $\delta \simeq 1$), an aver-

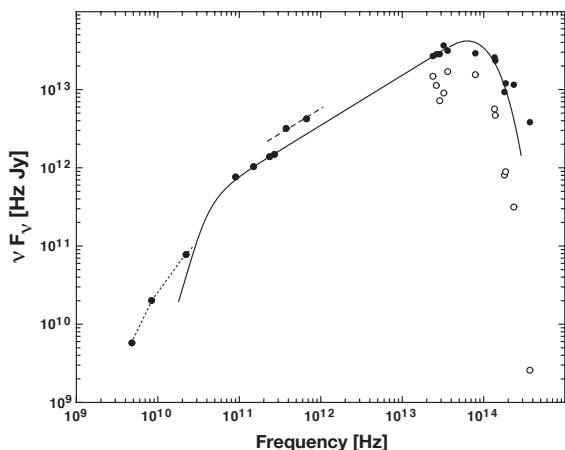


Fig. 21. Overall spectrum of the core of Centaurus A. Open circles show observed flux values, filled dots are corrected for the foreground extinction of $A_V = 14$ mag. The synchrotron spectrum (solid line) shows an optically thin power-law $F_\nu \sim \nu^{-0.36}$ which cuts off exponentially at $\nu_c = 8 \times 10^{13}$ Hz, and is self-absorbed below $\nu_1 \simeq 4.5 \times 10^{10}$ Hz. Evidence for variability exists around 3×10^{11} Hz (dashed line through photometry in 1991) and above ν_c (various epochs between 1997 and 2005). The excess at cm wavelengths ($\nu < 2 \times 10^{10}$ Hz, connected by dotted lines) is due to optical thick synchrotron components of larger size.

age magnetic field strength of $26 \mu\text{Tesla}$ (0.26 Gauß), and a maximum Lorentz factor $\gamma_{\text{max}} = 8500$ of the relativistic electrons responsible for the mid-infrared emission around ν_c . Our interferometric results on Centaurus A demonstrate that mid-infrared radiation processes are not restricted to thermal dust emission. Spectra which exponentially cut off towards short wavelengths do not necessarily represent the Wien tail of a blackbody spectrum, but are naturally expected from synchrotron sources as well.

The thermal dust emission from the core of Centaurus A is very feeble, more than 20 times weaker than that of the Circinus galaxy at the same distance. We think that both a lack of dust in the inner parsec and the absence of a sufficiently strong heating source are responsible for this. Certainly, Centaurus A does not contain a torus which blocks our line of sight onto a bright central accretion disk emitting optical and UV light. Most likely the accretion onto its black hole happens via an *advection dominated accretion flow* (ADAF), which is very inefficient in converting accretion power $\dot{m}c^2$ into radiation.

6. Outlook: observations of fainter, more distant AGN

The three active nuclei, Circinus, NGC 1068, and Centaurus A, which current MIDI observations have resolved well, are the closest and therefore brightest N-band sources in the southern sky. The challenge ahead is to extend this refined sample to a larger and more representative variety of AGN. Most importantly, the second aspect of the unified scheme has to be addressed: do Seyfert 1 galaxies indeed possess the same kind of dust tori as the Seyfert-2s? Un-

fortunately, the closest Seyfert 1 galaxy, NGC 4151, lies so far north that it rises just 25° above the horizon from Cerro Paranal. This makes observations in the mid-infrared very challenging⁸ and does not allow us to cover a reasonable part of the uv -plane. Thus we have to look out for more distant, fainter targets.

Although larger distances D imply smaller *scale factors* $s[\text{pc}] = 200 \text{ mas}/D[\text{Mpc}]$, and one would naturally expect that more distant AGN appear worse resolved, the situation is not such hopeless: one expects that the typical radius $r(T_d)$ of dust heated to the temperature T_d scales like $r(T_d) \propto L^{1/2}$, where L is the luminosity of the accretion disk. On the other hand, the luminosity is related to the observed flux F_{tot} by $L \propto F_{\text{tot}} \cdot D^2$. Thus, the apparent angular size of dust at temperature T_d is given by $\Delta(T_d) = s \cdot r(T_d) \propto D^{-1} L^{1/2} \propto F_{\text{tot}}^{1/2}$, independent of the distance D to the AGN. Accordingly, to first order we expect that the dust structures in all fainter AGN listed in Tab. 2 (with N-band fluxes between 300 and 650 mJy) have essentially the same apparent diameter at a wavelength of $\lambda = 12 \mu\text{m}$, which is dominated by the radiation from dust at $T_d = 300$ K.

6.1. The AGN snapshot survey with MIDI

In order to find all AGN which are suitable for observations with MIDI, the MIDI science team has initiated the *AGN snapshot survey* with MIDI. It is carried out in the guaranteed time of the consortium which built the MIDI instrument (see ESO Doc. No. VLTI-SCI-MID-15820-304, p. 3-16). The snapshot survey tries to get MIDI observations of 17 AGN, which are brighter than $S_N = 300$ mJy at $11.8 \mu\text{m}$ (listed in Tab. 2).

6.2. Exemplary results on distant AGN

In Figs 22 and 23 the MIDI snapshot results of two distant Seyfert galaxies are displayed. Using the shortest VLTI baseline UT2-UT3 the correlated flux $F_{\text{corr}} \gtrsim 0.4$ Jy well suffices to allow an accurate interferometric measurement. As explained in Sect. 2.3 the errors in F_{tot} by far exceed those in F_{corr} . Within those errors, F_{tot} and F_{corr} perfectly agree: the sources remain unresolved. The most promising strategy for resolving these faint, distant targets will compare various measurements of the correlated flux obtained with increasingly wider telescope separation. With the data at hand we can only state that MIDI is able to track fringes on the targets and propose observations with longer baselines.

As one can see in the column “MIDI” of Tab. 2, 11 out of the 15 AGN, for which MIDI observations have been attempted, led to a successful fringe detection. Three of the failures were due to the lack of a suitable AO reference

⁸ Note added in proof: In April 2008 we managed to observe and resolve NGC 4151 with MIDI.

Table 2

Target list and results of the AGN snapshot survey carried out during MIDI guaranteed time observations (GTO). Sources marked by * have been released early for observations during science demonstration time. A cross in the column ‘‘MIDI’’ indicates successful MIDI observations (X: complete interferometric measurement, x: fringes detected, but unstable weather conditions prohibited complete observation).

Name	Type	z	Scale [mas/pc]	$S_N(\text{core})$ [mJy]	MIDI	Remarks
*NGC 1068	S2	0.00379	14.0	15000	X	well observed (16 visibility points), see text
NGC 1365	S1.8	0.00546	11.0	610	X	marginally resolved in snapshot survey
IRAS 05189-2524	S2	0.0425	1.0	550		AO correction with MACAO failed
MCG-5-23-16	S1.9	0.00827	5.7	650	X	done in snapshot survey
Mrk 1239	S1	0.0199	2.5	640	X	done in snapshot survey
NGC 3281	S2	0.01067	4.4	620		AO failed on nucleus, nearby star not used
*NGC 3783	S1	0.00973	5.0	590	X	observed by Beckert et al. (<i>in prep.</i>)
NGC 4151	S1	0.00182	14.0	1400	X	resolved in snapshot survey
Centaurus A	RG	0.00332	53.0	1220	X	first results with short baselines, see text
IC 4329A	S1	0.01605	3.1	420	x	fringes detected
*Mrk 463	S1	0.0504	1.0	340		not yet tried
Circinus	S2	0.00145	50.0	9700	X	well observed (21 visibility points), see text
NGC 5506	S2	0.00618	8.0	910		AO correction with MACAO failed
NGC 7469	S1	0.01631	3.1	410	x	fringes detected
NGC 7582	S2	0.00539	9.0	320		
3C 273	QSR	0.1583	0.3	350v	X	one interferometric measurement
NGC 253 core	LE	0.00080	57.3	1100	–	no fringes detected (Hönig, <i>priv. comm.</i>)

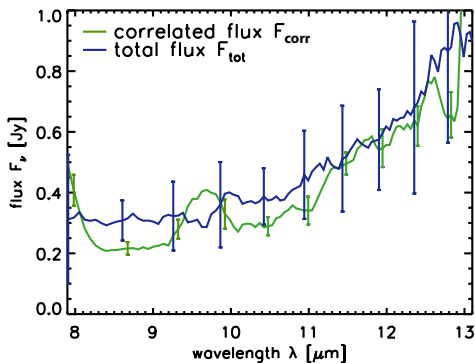


Fig. 22. Result of the MIDI snapshot survey for the distant Seyfert 2 galaxy MCG-5-23-16 (distance $D = 35$ Mpc). Both the total flux F_{tot} , and the correlated flux F_{corr} of the observation with the shortest VLTI baseline UT2–UT3 are shown. Since they agree within the errors, the source remains unresolved. Note the steep rise towards long wavelengths and the absence of a strong silicate absorption which is commonly seen in nearby Seyfert 2 galaxies.

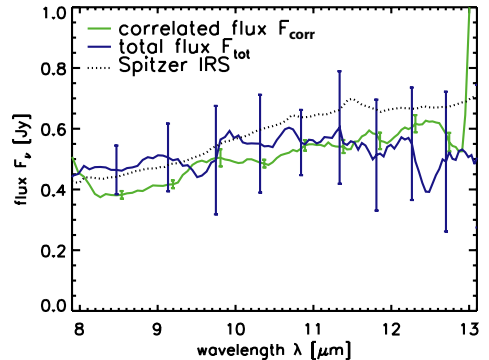


Fig. 23. Result of the MIDI snapshot survey for the distant Seyfert 1 galaxy Mrk 1239 ($D = 80$ Mpc). The total flux F_{tot} and the correlated flux F_{corr} of an observation with the shortest VLTI baseline UT2–UT3 are shown together with a spectrum observed with the Spitzer Space Telescope. Since they agree within the errors, the source remains unresolved. Note the almost flat spectral distribution which indicates a substantial contribution from the hot accretion disk, expected for a Seyfert 1 galaxy.

source (galaxy nucleus too diffuse and absence of a nearby reference star). The fourth failure is on NGC 253 which does not contain a strong AGN.

The most distant source for which MIDI detected fringes is the famous quasar 3C 273 at redshift $z = 0.158$. However, rather unstable weather conditions prevented us

from getting a photometric measurement. Since the well-measured correlated flux in the observing night (February 7, 2007) significantly exceeded both the typical flux values F_{tot} quoted in the literature and the photometric measurements with the mid-infrared instrument VISIR on Paranal obtained only three weeks later, it seems obvious that

we caught 3C 273 in an untypically bright phase, which certainly was dominated by the synchrotron emission of its blazar core. Measurements in a quiet phase would be required to resolve a thermal dust structure. It has to be seen whether MIDI is sensitive enough to allow such an observation.

6.3. The next steps

The team which carried out the MIDI guaranteed time program and the study of NGC 1068 (Walter Jaffe, David Raban and Huub Röttgering in Leiden, Konrad Tristram, Leonard Burtcher, Christoph Leinert, Uwe Graser and myself in Heidelberg) is also preparing the immediate next steps of AGN investigations with MIDI:

- Finish the investigation of the Circinus galaxy with MIDI, using longer baselines UT2-UT4 and UT1-UT3 and trying very short baselines provided by the ATs.
- Extend the study of NGC 1068, using the ATs in order to accomplish better uv -coverage.
- Resolve Centaurus A properly.
- Get a proper measurement of 3C 273, including simultaneous photometry.
- Try to resolve distant Seyfert 1 galaxies with the longest VLTI baselines.
- Observe more Seyfert 2 galaxies, in order to get a clearer picture which properties are special to Circinus and NGC 1068 and which are generic for Seyfert 2s.

Many of these observations are already scheduled in ESO's observing period 81 (April 1 to September 30, 2008).

7. The future: new instruments at the VLTI

The next major breakthrough in interferometric investigations of AGN can be expected when it will be possible to reconstruct *true images*. As Figs 16 and 17 demonstrate, we expect that the dust structure in AGN tori is extremely complex: modelling the observations by a few symmetrical components is certainly inadequate!

Fifty years of experience in radio interferometry have told us that the *phase* information (*i.e.* the information about the delays between the time when the wavefront from the source hits the different telescopes) is more important for image reconstruction than the mere correlated flux (which essentially contains the information of the coherence of the wavefront between the telescopes). Rapid variations of the diffractive index in the atmosphere generate random phase shifts between those parts of the wavefront which enter the different telescopes. Thus, the *intrinsic phase* information about the source structure is washed out. The problem is already present for radio observations at centimeter wavelengths. Therefore, radio astronomers had to develop a technique how to recover the phase information. Their method is called "self calibration" and essentially uses the fact that "closing" the relative observed phase shifts between each two telescopes on a triangle of three telescopes

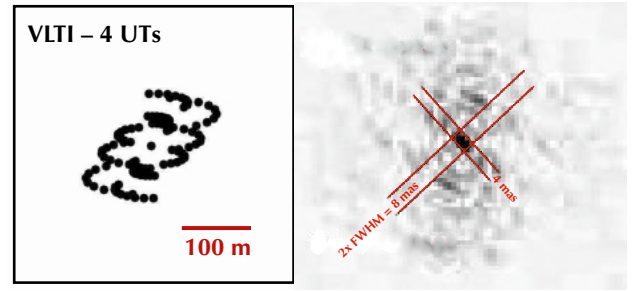


Fig. 24. The uv -coverage of the six possible UT combinations of the VLTI for a source at declination $\delta = -30^\circ$ (left) and image of a point source observed at $\lambda = 2 \mu\text{m}$ (referred to as "point spread function" or "dirty beam") observed with those configurations during one night. Pairs of parallel lines indicate the angular beam width $b = \lambda/B \simeq 2 \times \text{FWHM}$.

must lead to a sum $\phi_{12} + \phi_{23} + \phi_{31} = 0$ for the intrinsic phase. Thus, one can iterate the observed phases by assuming random offsets for each of the phases ϕ_{ij} until the "phase closure" sum vanishes. In practice, the method works best if there exists a rather strong point source in the field-of-view. See contribution by Monnier (2007) in the first volume of this series.

The minimum requirement for applying the phase closure technique is to record the interferometric signals of the combinations in between *at least three* telescopes simultaneously. Thus an interferometric instrument which combines three or more telescope beams is mandatory.

In the near infrared, the VLTI instruments AMBER (already working at the VLTI) and PRIMA (to be commissioned between 2008 and 2010 at the VLTI) offer the required three-beam capacity. The second-generation mid-infrared instrument MATISSE (planned for 2013) will allow the combination of three or four beams. In the following I will outline, which kind of AGN studies will be possible with these instruments.

7.1. AGN studies with the near-infrared instruments AMBER and PRIMA

The Astronomical Multiple BEam Recombiner (AMBER, see Petrov et al., 2003, and contribution by Markus Wittkowski in this book) allows one to combine the beam of three telescopes. Thus the closure phase method can be used for imaging. It operates in the near infrared ($1.1 \dots 2.5 \mu\text{m}$) and offers spectral resolutions $R = 30, 1500, \text{ and } 12000$. The imaging capabilities of AMBER are demonstrated in Fig. 24: using the two telescope triangles – [UT2-UT3, UT3-UT4, UT4-UT2], and [UT1-UT3, UT3-UT4, UT4-UT1] – could nicely cover the uv -plane of a target at $\delta = -30^\circ$ resulting in a point spread function with a core of $2 \text{ mas} \times 4 \text{ mas}$ (FWHM). AMBER observations of *e.g.* NGC 1365 (see Tab.2) could thus lead to images of the innermost, hottest parts of the dust distribution with a linear resolution of $\sim 0.3 \text{ pc}$.

Nevertheless, there exist two problems with employing AMBER for studies of AGN: In most cases, successful AGN

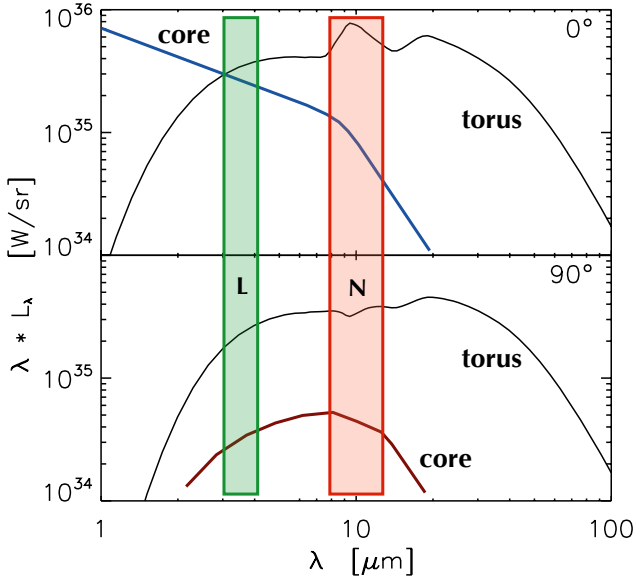


Fig. 25. The total spectra of Seyfert 1 ($i = 0^\circ$, upper panel) and Seyfert 2 galaxies ($i = 90^\circ$, lower panel) calculated for a clumpy torus model. The contribution from the hot accretion disk (core) and the torus are shown separately. Note that spectral luminosities, λL_λ , are given.

observations will require to reach a sensitivity of $K \gtrsim 10$ mag (60 mJy) in the correlated flux. AMBER could reach this only with the help of an additional fringe tracker, FINITO. But currently, AMBER plus FINITO do not reach fainter than $K \simeq 8$ mag, due to various problems of the VLTI infrastructure and in feeding the beams into the entrance fibers of AMBER. The second, more generic problem concerns the role of near-infrared emission from AGN: as one can see from the AGN model spectra in Fig. 25, the flux of the torus falls off very steeply short-wards of $2.5 \mu\text{m}$, even in the Seyfert 1 case ($i = 0^\circ$), in which an unobscured view on the hottest parts of the dust should be possible. The luminosity of a standard accretion disk is $> 10\times$ larger. Thus detecting the torus at $\lambda \lesssim 2 \mu\text{m}$ will require excellent dynamic range (> 100) between the central point source and the extended emission. On the other hand, in Seyfert 2 galaxies, both the emission from the hottest parts of the torus and the accretion disk are suppressed. But one knows from polarimetry of Seyfert 2 that light from the accretion disk and the Broad Line Region (BLR) is able to reach us via scattering. Thus, it could be difficult to distinguish dust emission and scattered light at near infrared wavelengths.

The Phase Referenced Imaging and Micro-arcsecond Astrometry Instrument (PRIMA, see contribution by F. Delplancke in this book) is a dual-feed instrument which allows to observe the target and a (brighter) reference star within $1'$ simultaneously. Phase measurements on the reference star also provide phase information for the target. The beams from the target do not need to be combined in PRIMA itself, but also can be fed into another instrument like AMBER and MIDI. In this way PRIMA offers a range of very promising observational tools for AGN research:

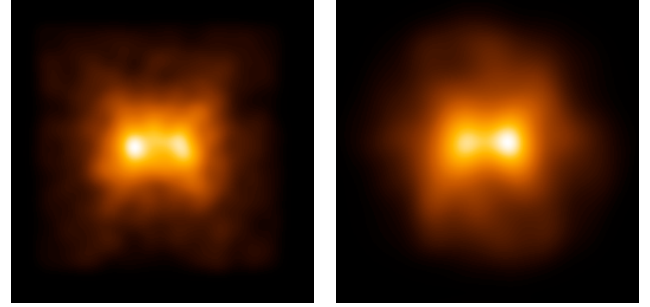


Fig. 26. Image reconstruction from observations with the second generation four-beam instrument MATISSE. The left panel shows an simulated image from the clumpy torus model of Hönig et al. (2006) at $\lambda = 3.6 \mu\text{m}$. The image is Fourier-transformed and the simulated visibilities are extracted on uv -tracks that simulate VLTI observations of Circinus ($\delta = -65^\circ$). They are modified with realistic photon noise. These “observed” visibilities are fed into the image reconstruction process foreseen for MATISSE. The reconstructed image is shown in the right panel (courtesy of K.-H. Hofmann, MPIfR Bonn).

- AGN close to a sufficiently bright reference star ($K < 12$) can be observed with the VLTI, independently of their correlated flux. Thus a range of very faint AGN become available (also for AMBER and MIDI).
- The phase referencing provides MIDI with the phase information for image reconstruction. In this way, also images of the torus in the mid-infrared will become available.
- The high-precision astrometry with respect to a reference star will allow one to relate the relative position of the near- and mid-infrared emission. based on the astrometric information scattered light and offsets between the hottest and cooler dust can be identified.

7.2. The second-generation mid-infrared instrument MATISSE

For the year 2013, it is planned to replace MIDI by the second-generation mid-infrared instrument MATISSE (= “Multi-AperTure mid-Infrared SpectroScopic Experiment”). MATISSE will not only offer full imaging capability by combining the beams from up to four telescopes, but also extend the accessible wavelength range by adding the L- (around $3.6 \mu\text{m}$) and M-band ($4.5 \mu\text{m}$) to the N-band ($10.5 \mu\text{m}$) used by MIDI. Simultaneous observations in the L- and N-band will be possible. In this way, images of both the hottest dust and cooler regions in the torus as well as their relative location can be obtained (Fig. 25). The wide wavelength range will allow one to determine the temperature distribution throughout the torus much more accurately. The L-band offers two additional advantages for AGN research: first, the angular resolution at $3.6 \mu\text{m}$ is three times better than that at $10.5 \mu\text{m}$ for a given baseline. Thus, the best MIDI resolution of ~ 10 mas will be improved to 3 mas, providing a much sharper view on the innermost regions of the torus (see simulation in Fig. 26). Second, the background from the atmosphere and the VLTI

is much lower in the L-band. Therefore, one expects that about 50 AGN will be accessible for mid-infrared interferometry by fringe tracking in the L-band and simultaneous integration in the N-band.

The most exciting prospect of MATISSE observations is not only that the fine structure of the inner torus can be investigated but also temporal variations – due to moving clouds or variations of the illumination by the accretion disk – might become detectable during a time span of several years. Thus, with some patience even dynamical information about the dust structure might become available.

8. Summary

The observations of the mid-infrared emission from the central parsecs of AGN with MIDI at the VLTI have already provided a wealth of new information. The AGN heated dust structure in the closest Seyfert 2 galaxies appears rather complex: the highest density parts form a geometrically thin (disk- or sheat-like) structure which is confined to a few times the dust sublimation radius. In the two well-observed cases – Circinus and NGC 1068 – it is related to the location of water masers. It is embedded into a geometrically thick distribution of warm dust ($T_d \simeq 300$ K) which can be identified as the AGN heated part of the torus. At least in the Circinus galaxy, there is clear evidence that this extended dust “torus” is not smoothly filled with dust (and gas), but consists of clumps or filaments which allow the UV-optical radiation from the core to penetrate little attenuated over several parsecs into the torus. From the depth of the silicate feature we conclude that about 50% of the total dust column towards the core is enclosed within the “surface” of warm dust emission. Notably, the extended dust distribution appears rather round, such that the definition of a “torus axis” has to rely on the inner, geometrically thin dust structure. Rather confusingly, this axis agrees well with that of large-scale outflow phenomena only in one of the two cases. A significant misalignment is present in NGC 1068.

Although the observations of Seyfert 2s are in general agreement with the expectations from the unified scheme, it is too early to draw final conclusions, before it will be established by future observations that Seyfert 1 galaxies contain the same kind of dust structures. The AGN snapshot survey has already established that several Seyfert 1 galaxies allow fringe tracking with MIDI. Using the longest baselines of the VLTI should suffice to resolve the expected dust tori in these more distant AGN as well.

The MIDI observations of the closest strong radio galaxy, Centaurus A show no evidence of a thick dust torus which could block the light from the core. Instead, the mid-infrared emission of Centaurus A is dominated by a non-thermal point source, that is surrounded by a rather feeble dust distribution. The later might represent a thin disk, the axis of which coincides with the parsec-scale radio jets. This excludes the possibility that Centaurus A contains a dust-

enshrouded, luminous accretion disk. In this type of AGN accretion onto the super-massive black hole takes place in the form of a radiatively inefficient process.

Significant further progress is expected in the next couple of years: the observations of about 10 fainter and more distant AGN which are within the reach of MIDI will increase the statistic and so enable us to distinct between source specific and generic properties. Phase referencing with PRIMA will open up a new window on faint AGN (which happen to lie near a suitable reference star). The most spectacular breakthrough will come with the advent of imaging: it cannot be excluded that the first true mid-infrared images of dust tori do neither look like the simple observational models (*e.g.* Fig. 11), nor like the simulated torus images (Fig. 16) and thus force us to revise our current concepts about the dusty tori in AGN substantially.

Acknowledgements: The MIDI investigations on AGN have been carried out in close collaboration with Konrad Tristram, Walter Jaffe, David Raban and Huub Röttgering. But many more people play an important role in the success: Leonard Burtscher, Bill Cotton, Uwe Graser, Thomas Henning, Christoph Leinert, Bruno Lopez, Guy Perrin (of the MIDI GTO team), and Sebastian Morel, Andrea Richichi, Markus Wittkowski (ESO VLTI team). The torus models have been developed with Marc Schartmann, Max Camenzind, Sebastian Wolf, Hubert Klahr and Thomas Henning.

Especially, I would like to thank Konrad Tristram and Leonard Burtscher, who carefully read the manuscript and improved it by many suggestions.

References

- Camenzind, M., 1995. Magnetic Fields and the Physics of Active Galactic Nuclei. In: Klare, G. (Ed.), *Reviews in Modern Astronomy*. Vol. 8 of *Reviews in Modern Astronomy*. pp. 201–234.
- Chesneau, O., Oct. 2007. MIDI: Obtaining and analysing interferometric data in the mid-infrared. *New Astronomy Review* 51, 666–681.
- Gallimore, J. F., Baum, S. A., O’Dea, C. P., Oct. 2004. The Parsec-Scale Radio Structure of NGC 1068 and the Nature of the Nuclear Radio Source. *ApJ* 613, 794–810.
- Greenhill, L. J., Booth, R. S., Ellingsen, S. P., Herrnstein, J. R., Jauncey, D. L., McCulloch, P. M., Moran, J. M., Norris, R. P., Reynolds, J. E., Tzioumis, A. K., Jun. 2003. A Warped Accretion Disk and Wide-Angle Outflow in the Inner Parsec of the Circinus Galaxy. *ApJ* 590, 162–173.
- Häring-Neumayer, N., Cappellari, M., Rix, H.-W., Hartung, M., Prieto, M. A., Meisenheimer, K., Lenzen, R., May 2006. VLT Diffraction-limited Imaging and Spectroscopy in the NIR: Weighing the Black Hole in Centaurus A with NACO. *ApJ* 643, 226–237.

- Hönig, S. F., Beckert, T., Ohnaka, K., Weigelt, G., Jun. 2006. Radiative transfer modeling of three-dimensional clumpy AGN tori and its application to NGC 1068. *A&A* 452, 459–471.
- Jaffe, W., Meisenheimer, K., Röttgering, H. J. A., Leinert, C., Richichi, A., Chesneau, O., Fraix-Burnet, D., Glazeborg-Kluttig, A., Granato, G.-L., Graser, U., Heijligers, B., Köhler, R., Malbet, F., Miley, G. K., Paresce, F., Pel, J.-W., Perrin, G., Przygodda, F., Schoeller, M., Sol, H., Waters, L. B. F. M., Weigelt, G., Woillez, J., de Zeeuw, P. T., May 2004. The central dusty torus in the active nucleus of NGC 1068. *Nature* 429, 47–49.
- Jaffe, W. J., Oct. 2004. Coherent fringe tracking and visibility estimation for MIDI. In: Traub, W. A. (Ed.), *New Frontiers in Stellar Interferometry*, Proceedings of SPIE Volume 5491. Edited by Wesley A. Traub. Bellingham, WA: The International Society for Optical Engineering, 2004., p.715.
- Kellermann, K. I., Zensus, J. A., Cohen, M. H., Feb. 1997. A New Limit to the Size of the Radio Nucleus of NGC 5128. *ApJ* 475, L93.
- Klahr, H. H., Henning, T., Kley, W., Mar. 1999. On the Azimuthal Structure of Thermal Convection in Circumstellar Disks. *ApJ* 514, 325–343.
- Krolik, J. H., Begelman, M. C., Jun. 1988. Molecular tori in Seyfert galaxies - Feeding the monster and hiding it. *ApJ* 329, 702–711.
- Leinert, C., Oct. 2004. Scientific observations with MIDI on the VLTI: present and future. In: *New Frontiers in Stellar Interferometry*, Proceedings of SPIE Volume 5491. Edited by Wesley A. Traub. Bellingham, WA: The International Society for Optical Engineering, 2004., p.19.
- Leinert, C., Graser, U., Waters, L. B. F. M., Perrin, G. S., Jaffe, W., Lopez, B., Przygodda, F., Chesneau, O., Schuller, P. A., Glazeborg-Kluttig, A. W., Laun, W., Ligi, S., Meisner, J. A., Wagner, K., Bakker, E. J., Cotton, B., de Jong, J., Mathar, R., Neumann, U., Storz, C., Feb. 2003. Ten-micron instrument MIDI: getting ready for observations on the VLTI. In: *Interferometry for Optical Astronomy II*. Edited by Wesley A. Traub. Proceedings of the SPIE, Volume 4838, pp. 893-904 (2003).
- Meisenheimer, K., Tristram, K. R. W., Jaffe, W., Israel, F., Neumayer, N., Raban, D., Röttgering, H., Cotton, W. D., Graser, U., Henning, T., Leinert, C., Lopez, B., Perrin, G., Prieto, A., Aug. 2007. Resolving the innermost parsec of Centaurus A at mid-infrared wavelengths. *A&A* 471, 453–465.
- Monnier, J. D., Oct. 2007. Phases in interferometry. *New Astronomy Review* 51, 604–616.
- Petrov, R. G., Malbet, F., Weigelt, G., Lisi, F., Puget, P., Antonelli, P., Beckmann, U., Lagarde, S., Lecoarer, E., Robbe-Dubois, S., Duvert, G., Gennari, S., Chelli, A., Dugue, M., Rousset-Perraut, K., Vannier, M., Mourard, D., Feb. 2003. Using the near infrared VLTI instrument AMBER. In: Traub, W. A. (Ed.), *Interferometry for Optical Astronomy II*. Edited by Wesley A. Traub. Proceedings of the SPIE, Volume 4838, pp. 924-933 (2003). Vol. 4838 of Presented at the Society of Photo-Optical Instrumentation Engineers (SPIE) Conference. pp. 924–933.
- Raban, D., Jaffe, W., Röttgering, H. J. A., Meisenheimer, K., Tristram, K., Apr. 2008. Resolving the obscuring torus in NGC 1068 with the power of IR interferometry: Revealing the inner funnel of dust, *MNRAS* in preparation.
- Schartmann, M., Mar. 2007. Models of Dust and Gas Tori in Active Galactic Nuclei. Ph.D. thesis, Max-Planck-Institute for Astronomy, Heidelberg, Germany.
- Schartmann, M., Meisenheimer, K., Camenzind, M., Wolf, S., Henning, T., Jul. 2005. Towards a physical model of dust tori in Active Galactic Nuclei. Radiative transfer calculations for a hydrostatic torus model. *A&A* 437, 861–881.
- Schartmann, M., Meisenheimer, K., Camenzind, M., Wolf, S., Tristram, K. R. W., Henning, T., Feb. 2008a. Three-dimensional radiative transfer models of clumpy tori in Seyfert galaxies. *ArXiv:0802.2604*
- Schartmann, M., Meisenheimer, K., Klahr, H., Camenzind, M., Wolf, S., Henning, T., Apr. 2008b. Resolving the obscuring torus in NGC 1068 with the power of IR interferometry: Revealing the inner funnel of dust, *A&A* in preparation.
- Tristram, K. R. W., Oct. 2007. Observations of AGN with MIDI. *New Astronomy Review* 51, 717–723.
- Tristram, K. R. W., Meisenheimer, K., Jaffe, W., Schartmann, M., Rix, H.-W., Leinert, C., Morel, S., Witkowski, M., Röttgering, H., Perrin, G., Lopez, B., Raban, D., Cotton, W. D., Graser, U., Paresce, F., Henning, T., Nov. 2007. Resolving the complex structure of the dust torus in the active nucleus of the Circinus galaxy. *A&A* 474, 837–850.
- Wilson, A. S., Shopbell, P. L., Simpson, C., Storchi-Bergmann, T., Barbosa, F. K. B., Ward, M. J., Sep. 2000. Hubble Space Telescope Imaging of the Circinus Galaxy. *AJ* 120, 1325–1341.
- Wolf, S., Nov. 2001. Inverse raytracing based on Monte-Carlo radiative transfer simulations. *A&A* 379, 690–696.